APPLICATION OF GLOBAL OPTIMISATION ALGORITHMS TO MULTI-ROTOR SYSTEMS

Dima Usov, dmitrij.usov@manchester.ac.uk, University of Manchester (UK)
Timotheos Chronis, timotheos-georgios.chronis@manchester.ac.uk, University of Manchester (UK)
Antonio Filippone, A.Filippone@manchester.ac.uk, University of Manchester (UK)
Nicholas Bojdo, nicholas.bojdo@manchester.ac.uk, University of Manchester (UK)

Abstract

The presented study proposes a novel method for optimising rotors' position in a generic, non-overlapping multi-rotor system. The approach uses global optimisation algorithms with an objective function based on a recently developed low-order aerodynamic model for rotor-on-rotor interference "RORI". Two classical optimisation algorithms, Particle Swarm Optimisation and Genetic Algorithm, were used to ensure an algorithm-independent solution. The analysis was conducted on Twin-rotor, Tri-rotor and Tetra-rotor systems in a two-dimensional, unbounded optimisation space at a constant operating point. The results indicated that the best available minimum of the power ratio existed when rotors were reassembled into an inverse V-shaped formation pattern. The performance assessment of optimisation algorithms revealed that the Particle Swarm Optimisation outperformed the Genetic Algorithm in terms of mean execution time and solution repetitiveness for a given optimisation problem. The comparison against the Free-Vortex Wake model showed an agreement within 5% across all verification cases, indicating the potential of the proposed approach.

1. INTRODUCTION

In recent years, Urban Air Mobility (UAM) has received high attention levels. Numerous engineering startups and industry giants are competing to create a novel, electrically powered VTOL aircraft type suitable for intra-city operations to address future UAM market demands. A wide range of engineering problems must be addressed before eVTOL becomes a realistic class of air vehicles [1]. One of those concerns is associated with the propulsion system configuration design. The multi-rotary nature of these aircraft features a complex aerodynamic interference, affecting the propulsion system performance. The aerodynamic interaction between rotors could lead to overall system performance benefit or penalty depending on the relative rotor placement.

The number of potential rotor arrangements creates a vast space of configuration designs. Recent studies on multi-rotor interference mainly focused on pre-defined configurations of twin- and tetra-rotor systems [2-11]. However, the design-space exploration of arbitrary multi-rotor has received scarce attention in the literature. Traditional aerodynamic analysis tools that capture mutual interference effects between rotors (such as CFD and FVW analysis) are computationally expensive. Therefore, these traditional methods are impractical for solving problems that involve large design domains.

This work focuses on design-space reduction using a low-order aerodynamic interference analysis model combined with global optimisation algorithms. The methodology presented in the study reduces the global domain to a local domain of potential configurations of interest. It enables higher-fidelity exploration toward the optimal performance configuration of arbitrary multi-rotor systems. Due to the non-deterministic nature of global optimisation algorithms, two optimisation algorithms were used to verify that the solution is independent of a selected algorithm. Further, the study compared two optimisation approaches in terms of repeatability of the best available solution and computational time.

2. ANALYSIS

2.1. Aerodynamic Interference Model

The aerodynamic performance of the multi-rotor system was estimated based on the Rotor-On-Rotor Interference (RORI) model. The RORI model is a recently developed aerodynamic analysis tool for preliminary design and design space exploration purposes. A detailed explanation of the theory behind the RORI model and verification of performance predictions against free-vortex wake simulations is provided in Ref. [12]. In brief, the RORI model is based on a hybrid theory approach, where self-induced velocities and influence-induced velocities are estimated using generalised dynamic wake inflow and prescribed wake, respectively. The total induced velocity is obtained by superimposing self-induced and influence-induced inflows. The process is repeated until all inflow states reach convergence criteria. The model's flowchart is shown in Figure 1.

The RORI model's computational time was faster by two-to-three orders of magnitude compared to the FVW simulation (depending on the FVW code architecture),

Presented at 48th European Rotorcraft Forum, Switzerland, 6-8th September, 2022

while a relative difference in performance predictions was around 5%, which was sufficiently accurate for the scope of the current work. However, due to the limitations of the Beddoes prescribed wake, the RORI model does not apply to purely axial flight regimes nor low advancing ($\mu_\infty < 0.15$) edgewise flights [13]. Moreover, the model's performance predictions were not assessed for overlapping rotor cases. Hence, overlapping rotor cases will not be assessed in this work.

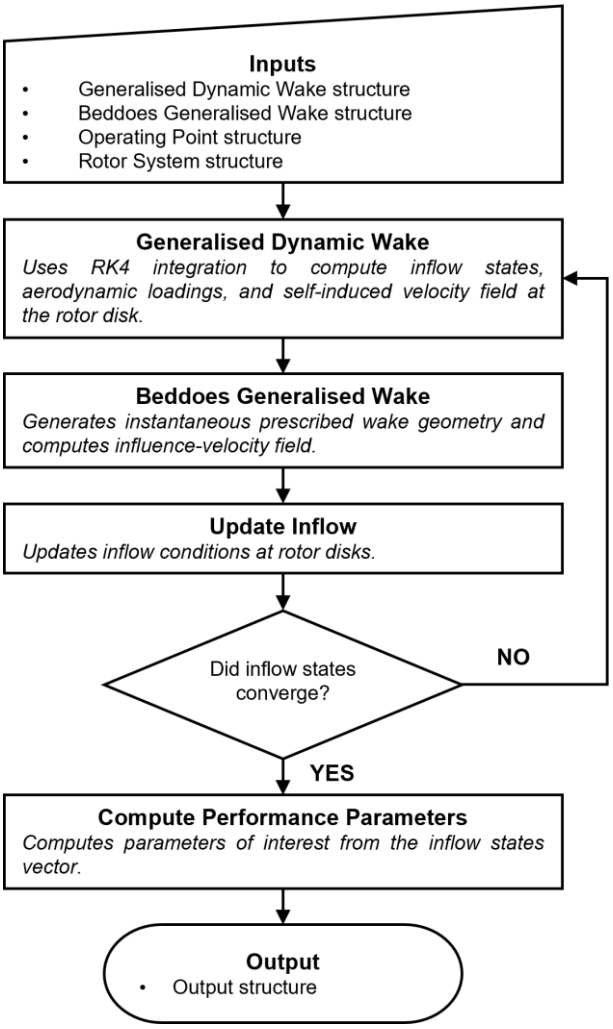

Figure 1: RORI model flowchart, adapted from [12].

2.2. Multi-rotor System

All rotors in the multi-rotor system were assumed to be identical, operating at the same angular speed and collective pitch setting angle. The only difference was the direction of the rotors' rotation, $\hat{\omega}_n$, where odd rotors were rotating anti-clockwise, and even rotors were rotating clockwise, e.g.,

$$\hat{\omega}_{\mathrm{n}} = \begin{cases} 1, & \text{for } n\ odd \\ -1, & \text{for } n\ even \end{cases} \tag{1}$$

Rotor geometries comprised two rectangular shape blades with a constant sectional blade chord $c/R = 0.093$ and a constant NACA 0012 aerofoil profile along the radius of the blade. The pre-cone angle was set to zero, the root cut-out was placed at $0.1R$, and the rotorspeed was constant at 589 rpm throughout all operating cases. The twist distribution was based on an XV-15 rotor blade and fitted by a fifth-order polynomial found in Ref. [14]. The aerodynamic characteristics of the NACA 0012 airfoil at $Re = 2 \times 10^6$ were modelled using linear aerodynamics theory with a lift-curve slope $c_{l,\alpha} = 5.73\, rad^{-1}$ and maximum lift coefficient of $c_{l,max} = 1.40$ [15]. The viscous losses were accounted for using a form of Bailey's drag polar for NACA 0012 airfoil, e.g.,

$$c_d = 0.0084 - 0.0102\alpha + 0.384\alpha^2 \tag{2}$$

with a validity limit $\alpha < 11.2°$ [15]. A Reynolds number correction factor with an exponent of 0.20 was used based on the expected operational range of the Reynolds number [16].

The advance ratio was fixed to $\mu_\infty = 0.15$, and the rotor incidence angle was set to $\alpha_s = 5°$ relative to the incoming flow, as shown in Figure 2. All rotors were set to a fixed collective pitch of $\theta_c = 7°$ and rotors' performance was allowed to vary under the influence imposed by the mutual aerodynamic interference effects in the rotor system.

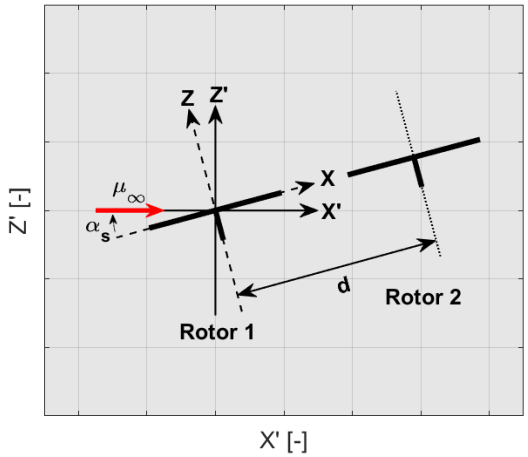

Figure 2: Definition of the rotor-system geometry.

2.3. Global Optimisation

Typically, a global optimisation algorithm would evaluate the objective function $10^2 - 10^6$ times, depending on the number of input variables and hyperparameter selection (e.g., particle swarm size, maximum iteration, social adjustment). The evaluation time of a single performance point of a multi-rotor using the RORI model was sufficiently small. It practically allowed to formulate the model as an objective function and execute a global optimisation algorithm to search for the domain of interest.

For this project's scope, the objective function took coordinates of rotors' hubs as input variables and output the total power ratio of a multi-rotor system as an objective parameter. The total power ratio is defined as

$$P_R = \sum \mathrm{C_P} / (C_{P,iso}\, N_R) = fval \tag{3}$$

and the total thrust ratio is

Presented at 48th European Rotorcraft Forum, Switzerland, 6-8th September, 2022

(4) $$T_R = \sum \mathrm{C_T} / (C_{T,iso}\, N_R)$$

The optimisation problem was compiled in a MATLAB® environment using MathWorks® native Global Optimization Toolbox.

Due to the non-deterministic nature of global optimisation algorithms, it is vital to ensure that the solution is repeatable and independent of a selected algorithm. Two classical global optimisation methods were used for the algorithm-independence study: Particle Swarm Optimisation (PSO) and Genetic Algorithm (GA). A detailed explanation of these global optimisation algorithms is summarised in Ref. [17, 18]. Each algorithm was run multiple times to check for the reproducibility of a solution. Before each run, the random number generator was reshuffled to ensure random initial conditions at the start of the algorithm. The jobs were run on independent nodes using High Throughput Computing (HTC) facility HTCondor at the University of Manchester to split the computational costs. Further, the computed data was analysed, and algorithm performance was compared against each other. Table 1 provides a summary of optimisation cases considered in this work. A single tetra-rotor GA optimisation output was lost during the data transfer. Considering the mean execution time, it was decided to omit an extra optimisation run, as it is statistically insignificant.

Table 1: Optimisation cases.

Rotor-System	***nvars***	***PSO Runs***	***GA Runs***
Twin	2	500	500
Tri	4	500	500
Tetra	6	499	499

The number of input variables was reduced by setting the first rotor to an origin position and varying the coordinates of the other rotors within the optimisation space. Due to the RORI model's limitations, the minimum distance between adjacent rotors' hubs was limited to 2.25 radii. When this condition was not satisfied, the penalty was applied to the objective value without evaluating the fitness function.

3. RESULTS

3.1. Optimisation cases

3.1.1 Twin-rotor

Typically, the true minima in the optimisation domain are unknown, and the optimisation solution cannot be compared against it. Therefore, the initial analysis was accomplished for a twin-rotor system in a two-dimensional, unconstrained optimisation space. This simplification allowed to evaluate the objective parameter in the entire optimisation domain using brute computational force prior to executing optimisation algorithms. Further, the optimisation solution was mapped on the pre-computed contour of the objective parameter. The difference between an optimisation solution and true minima in the given domain was examined, which would not be possible using a "blind" optimiser run.

The contour plot was generated by evaluating the fitness function throughout the entire sweep of coordinates defined in the domain in 0.01 increments. Further, GA and PSO were executed 500 times each, using independent nodes on the HTCondor facility and reshuffling the random number generator prior to each run. Finally, a set of solutions was obtained and mapped on the pre-computed contour plot and represented in Figure 3.

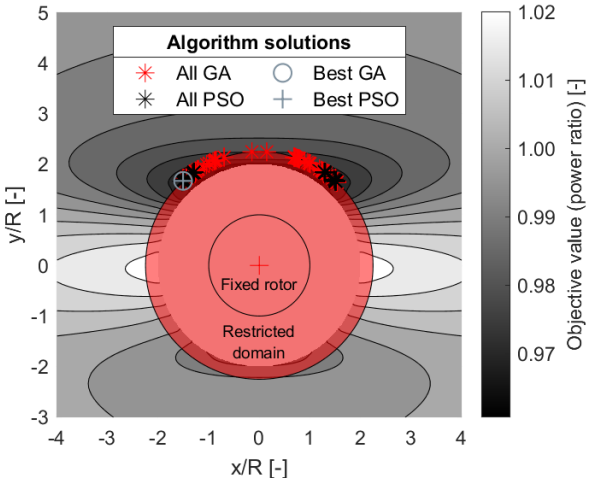

Figure 3: Contour plot of pre-computed objective parameter with mapped optimisation solutions.

In agreement with the pre-computed results, the optimisation results suggested that the twin-rotor configuration had global minima of an objective parameter, $fval = 0.9705$ when the free rotor hub was placed at $[-1.51, 1.67]$. Two global minima were expected due to the rotor system's lateral symmetry (Y-axis). The second global minimum was located at $[1.51, 1.67]$. The obtained solution of a twin-rotor configuration also agreed with the findings in Ref. [6, 12, 19].

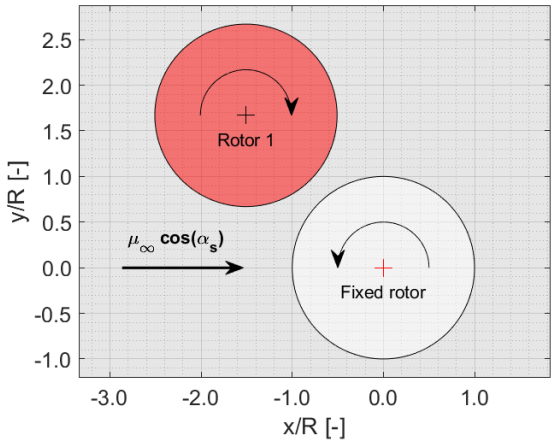

Figure 4: Best available twin-rotor configuration.

The configuration corresponding to the best available fval (minimum power ratio) is shown in Figure 4. In the optimal configuration, the rotors were in proximity from the

Presented at 48th European Rotorcraft Forum, Switzerland, 6-8th September, 2022

advancing sides. The advancing side of the downstream rotor (fixed rotor) was exposed to a predominant upwash created by the advancing side of the upstream rotor (rotor 1). The upstream rotor was also exposed to an upwash from the downstream rotor, but this effect was minor. The primary effect of an increased upwash is a decrease in local inflow angle ϕ, which leads to a forward tilt of a sectional lift vector along the blade radius, decreasing the torque and increasing the thrust [12], whereas the downwash results in the opposite effect. In the shown configuration, the aerodynamic interference between the rotors resulted in a net benefit to the twin-rotor system performance, reducing the power. If the downstream rotor were placed behind the retreating side of the upstream rotor, it would reduce the net performance benefit, as shown in Figure 14 for $240^\circ \leq \beta \leq 300^\circ$. Contrary to the fixed wing, the trailed vortex circulation of a rotary wing is periodic, reaching minima and maxima at blade azimuth angles $\psi_b = 270^\circ$ and $\psi_b = 90^\circ$, respectively. Therefore, the downstream rotor would experience a stronger upwash if positioned downstream to the advancing side of the upstream rotor.

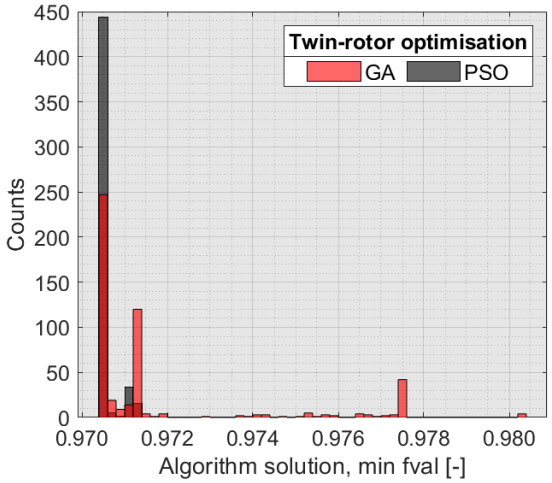

Figure 5: Histogram plot of algorithms solutions from independent nodes for twin-rotor system optimisation.

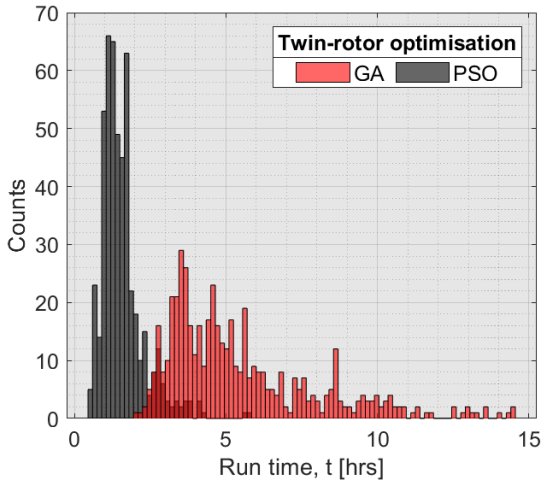

Figure 6: Histogram plot of algorithms evaluation time from independent nodes for twin-rotor system optimisation.

The performance of selected algorithms was evaluated in terms of the reproducibility of a solution and the execution time. Figure 5 shows a histogram comprising a complete set of optimisation results from 500 runs. The horizontal axis represents the value of the best optimisation solution from an independent run, and the vertical axis represents the count of repetitive solutions (the number of times a specific solution was obtained). According to the results, both GA and PSO converged to one of the two global minima ($fval = 0.9705$) in the $\sim 49\%$ and $\sim 89\%$ of the runs, respectively. However, the PSO algorithm demonstrated a better reproducibility of global minima than GA.

Figure 6 shows the computation time required to run an algorithm on an independent node. The results suggested that the mean execution time of a single run for the PSO was around 1 hour 34 minutes, whereas on average, it took 5 hours 29 minutes to run a single GA case.

3.1.2 Tri-rotor

The optimisation results of a tri-rotor system suggested that the best-known minima of a fitness function value, $fval = 0.9494$, was reached when the free rotors' hubs were placed at $[-1.53, 1.65;\ -1.30,\ -1.83\ ]$.

The best available tri-rotor configuration in terms of power ratio is shown in Figure 7. Similarly to the twin-rotor case, the optimisation algorithm led to the downstream rotor being placed behind the advancing sides of both upstream rotors, resulting in an inverse-V formation. It is worth noting that this tri-rotor configuration is not symmetric about the x-axis. This is likely due to the non-symmetric nature of rotor loading and rotation effects but requires further investigation.

The reproducibility performance of selected algorithms is shown in Figure 8. According to the results, the PSO solution converged to the best-known minimum ($fval = 0.9494$) in $\sim 63\%$ of runs. On the other hand, GA managed to find the best-known minimum objective parameter only in $\sim 9\%$ of all runs. The mean execution time results suggested that it took 7 hours 56 minutes for a single PSO run, while an average completion time for a single GA run was 11 hours 28 minutes, as shown in Figure 9.

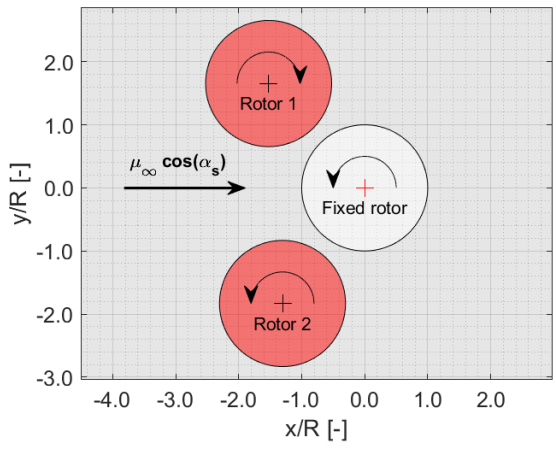

Figure 7: Best available tri-rotor configuration.

Presented at 48th European Rotorcraft Forum, Switzerland, 6-8th September, 2022

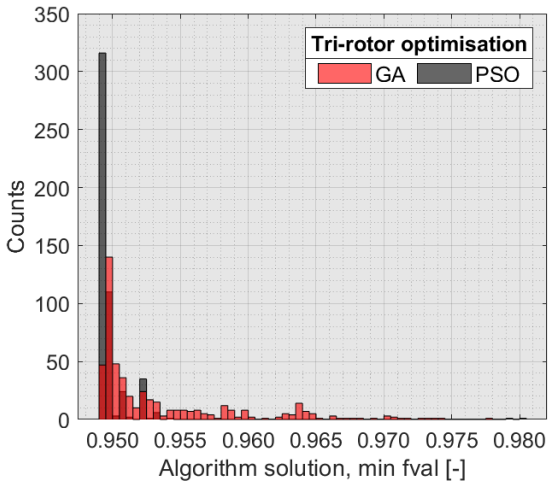

Figure 8: Histogram plot of algorithms solutions from independent nodes for a tri-rotor system optimisation.

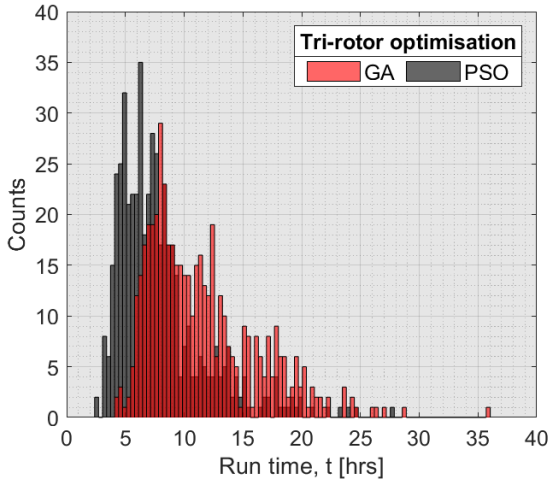

Figure 9: Histogram plot of algorithms evaluation time from independent nodes for a tri-rotor system optimisation.

3.1.3 Tetra-rotor

The optimisation solution of a tetra-rotor system indicated that the fitness function took its best-known minimum, $fval = 0.9349$ when the free rotors' hubs were positioned at $[-1.53, 1.65; -1.37, -1.79; -2.92, 3.42]$ as shown in Figure 10. In agreement with the twin-rotor and tri-rotor cases, the optimisation procedure placed downstream rotors behind the advancing sides of upstream rotors, forming the pattern of an inverse-V formation. Moreover, it can be noticed that the optimisation algorithm placed clockwise and anti-clockwise rotating rotors on the right and left branches of the inverse-V formation correspondingly. The same pattern was also observed for the tri-rotor case. If the inverse-V were viewed as a triangle with its sides passing through the rotors' hubs, the advancing sides of the rotors would be on the inside of the triangle. More work is required to determine if this pattern can be generalised.

The reproducibility of optimisation algorithms is shown in Figure 11. The GA and PSO solutions converged to the best-known minimum ($fval = 0.9349$) in ~32% and ~6% of all runs, respectively. Figure 12 shows that the mean computational time of a single PSO run was 16 hours 53 minutes, and a single GA run took 67 hours 11 minutes.

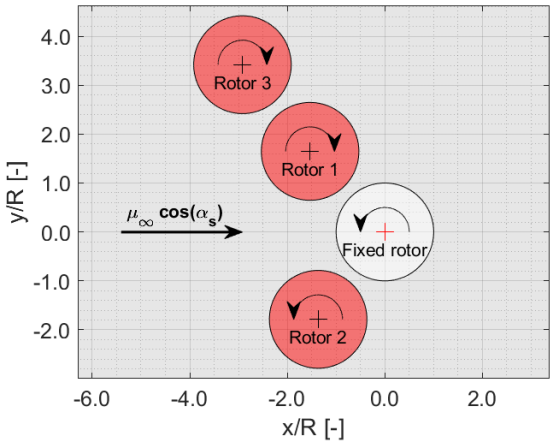

Figure 10: Best available tetra-rotor configuration.

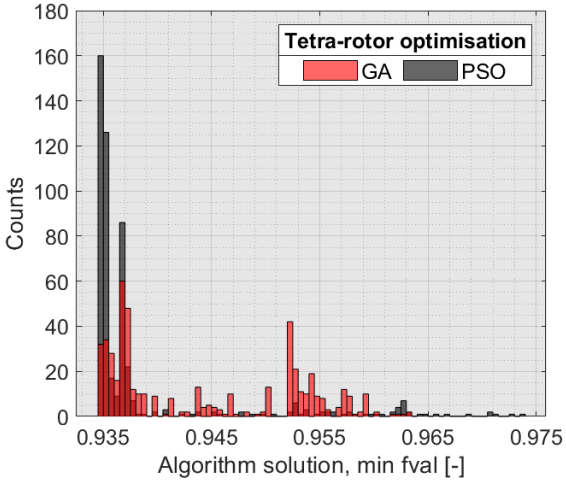

Figure 11: Histogram plot of algorithms solutions from independent nodes for a tetra-rotor system optimisation.

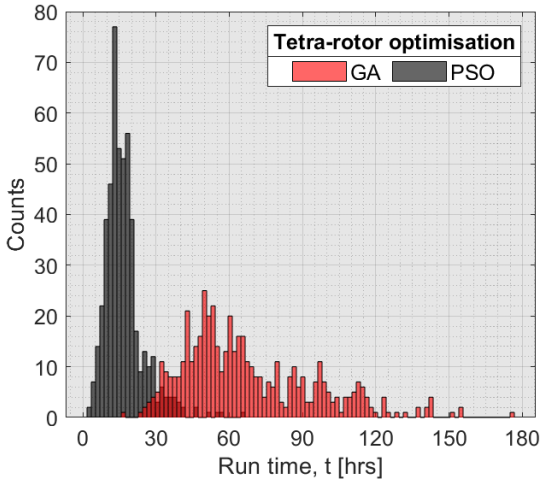

Figure 12: Histogram plot of algorithms evaluation time from independent nodes for a tetra-rotor system optimisation.

Presented at 48th European Rotorcraft Forum, Switzerland, 6-8th September, 2022

3.2. Verification

To verify the behaviour of the optimisation search, simulations were run using a free-vortex wake (FVW) model. This took the form of an object-oriented MATLAB® code developed at the University of Manchester as part of the UK Vertical Lift Network MENtOR project [20]. Details of the model's implementation can be found in a previous paper [12]. In brief, the model is derived from potential flow theory and represents the rotor blades and their wake as a lattice-like structure of vortex panels that are parsed into a series of connected vortex filaments. The vortex panels attached to the rotor blades are used to model the lifting properties of the blades, while the spatial positions of the wake nodes connecting the vortex filaments are free to move in time and space according to the instantaneous velocity field. In this work, first-order explicit integration of the wake node positions was used, with a dimensionless time step of fifteen degrees azimuth blade rotation. As the FVW model is an inviscid aerodynamic model, the viscous power component of the FVW results was taken from the generalised dynamic wake model.

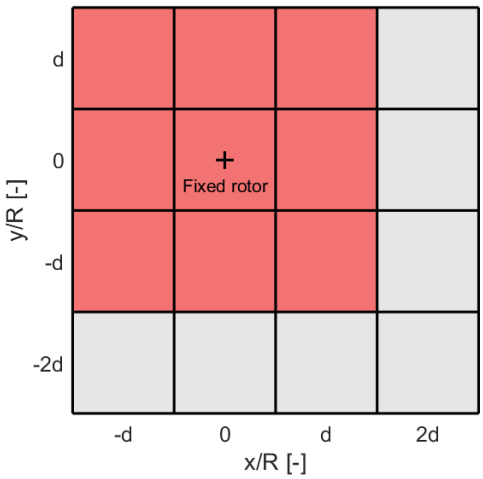

Figure 13: Grid for the selection of the random rotor configurations, $d = 2.25$. Tri-rotor configurations were taken from the shaded 3x3 grid, while tetra-rotor configurations were taken from the full 4x4 grid.

In the twin-rotor case, a sweep of relative hub-wind angles with a fixed hub-to-hub distance of 2.25R was simulated to directly verify the optima's location, as in Ref. [12]. In the tri- and tetra-rotor cases, random arrangements of the rotors were generated, the reasoning being that if the rotor system's performance predicted by both models matched sufficiently well for these random configurations, then it could be argued that an optimization search carried out with the FVW model would likely lead to the same optimal solution.

For the random configurations, uniform grids were used to define the locations of possible rotor placements, with the distance between grid-cell centres defined as 2.25 rotor radii, as shown in Figure 13. The first rotor was fixed to the same cell, while an algorithm was created to select random unique combinations from the remaining cells for the other rotors. The twelve configurations were sorted in descending order based on the power ratio predicted by the RORI model. The rotor coordinates for each one are given in Table 2 and Table 3 of the appendix (coordinates of rotor one are not given as they are always fixed at the origin). The same convention of alternating rotation directions was adopted for each configuration as in 2.2.

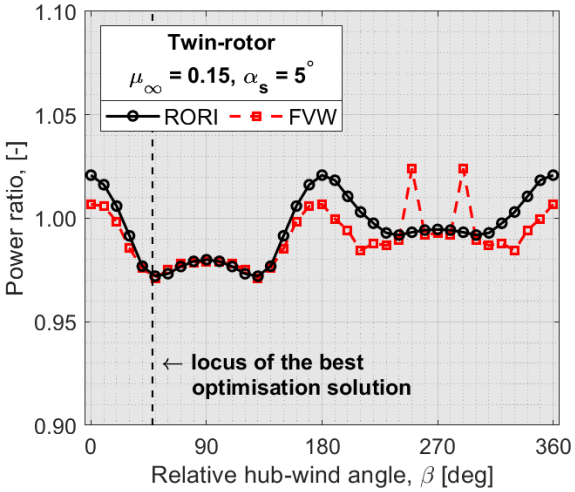

Figure 14: Power ratio of the twin-rotor system at different hub-wind angles, taken at 10° increments.

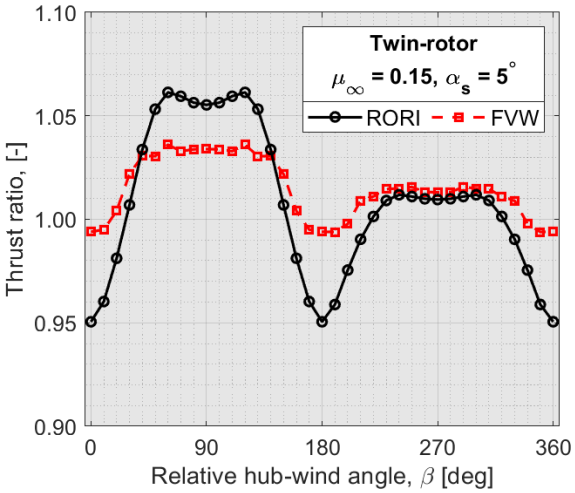

Figure 15: Thrust ratio of a twin-rotor system at different hub-wind angles, taken at 10° increments.

3.2.1 Comparisons

For the twin-rotor case in Figure 14, two outliers are noted in the power ratio predicted with the FVW model, at relative hub-wind angles of $\beta = 250°$ and $290°$. Examination of the instantaneous load history from these two cases revealed large fluctuations in the induced power coefficient of the downstream rotor, suggesting some instability in the simulations (this behaviour was also observed for configurations nine of both the tri- and tetra-rotor cases, marking these as potentially spurious results). This could be resolved by using a smaller timestep. With the exception of the two aforementioned angles, the power ratio of the two models is in good agreement, especially in the region of the minima, with a maximum difference of 1.88% and a mean of 0.72%. The locations of the minima

Presented at 48th European Rotorcraft Forum, Switzerland, 6-8th September, 2022

found by the optimisation are also confirmed as $\beta = 50°$ and $140°$.

In Figure 15, it can be seen that, although the differences in the thrust ratios are larger, the behaviour with respect to β still matches well, with a mean difference of 1.89% and a maximum of 4.37%.

The power and thrust ratios for the tri-rotor configurations are compared in Figure 16 and Figure 17. The power predictions match well in their general trend, with a mean difference of 0.81% and a difference of 1.10% for the best PSO configuration. Regarding the thrust predictions, it is noted again that the differences overall are larger, with a mean of 2.01%, but the shape is similar, with the FVW results showing a flatter trend.

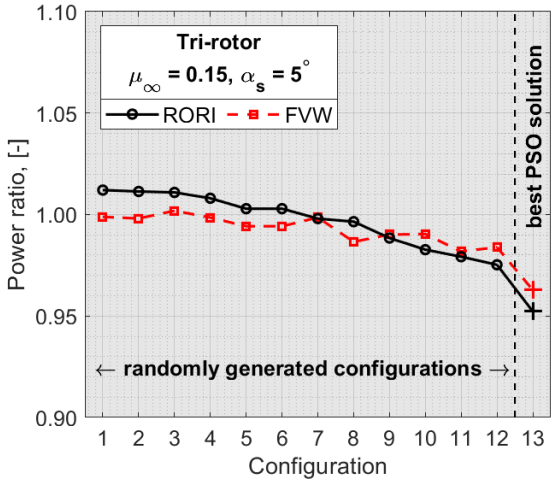

Figure 16: Power ratio of a set of tri-rotor systems.

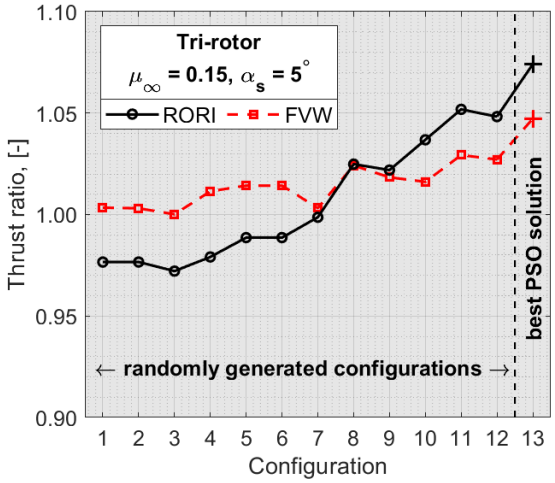

Figure 17: Thrust ratio of a set of tri-rotor systems.

For the tetra-rotor case, the power ratios show close agreement in Figure 18, with a mean difference of 0.76% between model predictions. Figure 19 shows that the thrust ratio predictions agree more closely than in the other cases, although the largest discrepancy of all cases is noted here for configuration one.

In all cases, the changes in system performance for the different configurations appear more pronounced in the RORI model predictions than in the FVW model. This behaviour was expected since the prescribed nature of the wake used by the RORI model does not account for any mutual interaction and therefore overpredicts the induced velocities on the other rotors [12]. This could be considered a beneficial feature from an optimisation standpoint as it may lead to faster convergence.

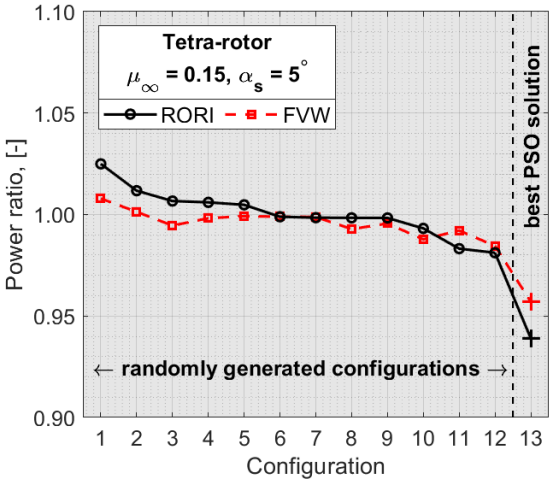

Figure 18: Power ratio of a set of tetra-rotor systems.

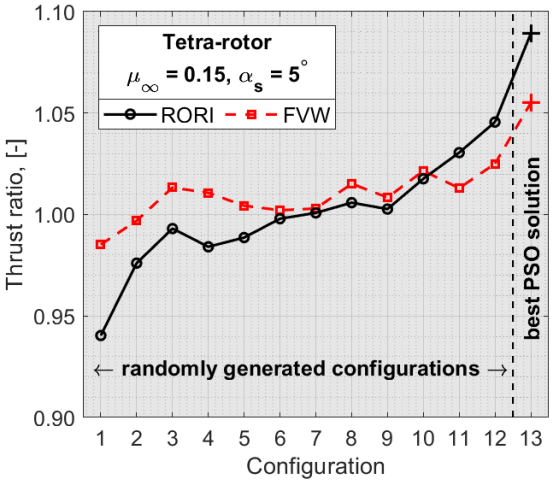

Figure 19: Thrust ratio of a set of tetra-rotor systems.

It is significant that, for the most part, the FVW predictions of the power ratio follow the same descending trend as the RORI model since, in optimisation, it is the relative values of the different design points that drive the search towards the optimum. The fact that the FVW model predicts the lowest power ratios for the best PSO configurations also gives confidence that the identified rotor arrangements are the best available and that the RORI model predicts the rotor interactions suitably well for a first-order analysis.

Comparing the two models in terms of computational cost, for a single rotor with two blades, the RORI model completed the evaluation in under two seconds, whereas the FVW model took on average 400 seconds, running on a single core with no explicit parallelisation. The difference would be greater were the FVW code not using MATLAB® executable (MEX) files to speed up the solution.

Presented at 48th European Rotorcraft Forum, Switzerland, 6-8th September, 2022

4. CONCLUSIONS

Two global optimisation algorithms, Genetic Algorithm and Particle Swarm Optimisation, attempted to search for the best power configuration of a hypothetical twin, tri, tetra-rotor system in a two-dimensional optimisation space. The performance of the algorithms was assessed based on the reproducibility of the best-available solution and a mean execution time. The objective function (fitness function) was formulated using the RORI model. The function took rotors hubs' coordinates as inputs and output the total power of the multi-rotor system at a given operating point.

In agreement with previous findings available in the literature, the results obtained suggested that in the minimum power configuration of a twin-rotor system, two existed when the rotors were placed diagonally with the advancing sides neighbouring each other. With the addition of more rotors, the inverse-V formation emerged as the optimal configuration. In all cases, the optimal solutions had the downstream rotors placed as close to each other as allowed behind the outboard of the advancing side of upstream rotors, suggesting this offers the maximum benefit from the mutual interactions. The inverse-V formation pattern can potentially be generalised as the minimum power configuration, but more evidence is required to verify this hypothesis.

The analysis verified that the optimisation solution was independent of the selected optimisation algorithm. The comparison between algorithms revealed that PSO outperformed GA in terms of the reproducibility of the best-known solution and computational time, provided both algorithms were run at MATLAB® default hyper-parameters. However, it is unclear if a tuning of algorithm-specific hyperparameters will affects the performance and, hence, the choice of the global optimisation algorithm.

In comparing with the FVW model, it was found that the two models agree within 2% in their prediction of the total power ratio in all cases, with the RORI model slightly overestimating the differences between configurations. The thrust ratio predictions are less in agreement but still within 5% for all configurations tested. Considering the computational saving of 2-3 orders of magnitude depending on the code architecture, the RORI model has shown promise in evaluating the interactional effects between two and more rotors.

ACKNOWLEDGEMENTS

This research is part-funded by the UK Research Councils (EPSRC) *Methods and Experiments for Rotorcraft* (Mentor), Grant EP/S010092/1, the UK Vertical Lift Network, EPSRC Grant EP/M018164/1, and a Presidential PhD Scholarship at the University of Manchester.

NOMENCLATURE

ABBREVIATIONS

CFD	*computational fluid dynamics*
eVTOL	*electric vertical take-off and landing*
FVW	*free-vortex wake*
GA	*genetic algorithm*
HTC	*high throughput computing*
PSO	*particle swarm optimisation*
RORI	*Rotor-on-Rotor Interference (model)*
RPM	*revolutions per minute*
VTOL	*vertical take-off and landing*
UAM	*urban air mobility*

GREEK SYMBOLS

α	=	*sectional angle of attack, [rad]*
α_s	=	*rotor incidence angle, positive tilted forward, [deg]*
β	=	*hub-wind angle, [deg]*
θ_c	=	*collective pitch setting angle, [deg]*
μ_∞	=	*free-stream advance ratio, $V_\infty/\Omega R$ [-]*
ρ	=	*air density, [kg m^{-3}]*
ϕ	=	*inflow angle, [rad]*
ψ_b	=	*blade azimuth angle, [deg]*
$\hat{\omega}$	=	*direction of rotor's rotation*
Ω	=	*rotorspeed, [rad s^{-1}]*

ROMAN SYMBOLS

A	=	*rotor disk area, πR^2 [m^2]*
c	=	*sectional blade chord normalised on R*
c_d	=	*blade's sectional profile drag coefficient*
$c_{l,\alpha}$	=	*blade's sectional lift-curve slope, [rad^{-1}]*
$c_{l,max}$	=	*maximum lift coefficient*
C_P	=	*time-averaged power coefficient, $P/\rho A(\Omega R)^3$*
C_T	=	*time-averaged thrust coefficient, $T/\rho A(\Omega R)^2$*
d	=	*hub-to-hub separation distance*
$fval$	=	*fitness function value*
N_R	=	*total number of rotors*
$nvars$	=	*number of input variables*
P	=	*rotor power, [W]*
P_R	=	*total power ratio*
R	=	*rotor radius, [m]*
Re	=	*Reynolds number*
T	=	*rotor thrust, [N]*
T_R	=	*total thrust ratio*
V_∞	=	*magnitude of free-stream velocity, [m s^{-1}]*
x, y	=	*coordinates in the global reference frame, [m]*

SUBSCRIPTS

iso	=	*isolated rotor*

Presented at 48th European Rotorcraft Forum, Switzerland, 6-8th September, 2022

REFERENCES

[1] A. Filippone and G. Barakos, "Rotorcraft systems for urban air mobility: A reality check," *The Aeronautical Journal,* vol. 125, no. 1283, pp. 3-21, 2021. DOI: 10.1017/aer.2020.52.

[2] E. J. Alvarez and A. Ning, "High-fidelity modeling of multirotor aerodynamic interactions for aircraft design," *AIAA Journal,* vol. 58, no. 10, pp. 4385-4400, 2020. DOI: 10.2514/1.J059178.

[3] D. Barcelos, A. Kolaei and G. Bramesfeld, "Aerodynamic interactions of quadrotor configurations," *Journal of Aircraft,* vol. 57, no. 6, pp. 1074-1090, 2020. DOI: 10.2514/1.C035614.

[4] P. V. Diaz and S. Yoon, "Computational study of NASA's quadrotor urban air taxi concept," in *AIAA SciTech 2020 Forum*, 2020. DOI: 10.2514/6.2020-0302.

[5] P. V. Diaz and S. Yoon, "High-fidelity computational aerodynamics of multi-rotor unmanned aerial vehicles," in *2018 AIAA Aerospace Sciences Meeting*, 2018. DOI: 10.2514/6.2018-1266.

[6] R. Duivenvoorden, M. Voskuijl, L. Morée, J. de Vries and F. van der Veen, "Numerical and experimental investigation into the aerodynamic benefits of rotorcraft formation flight," *Journal of the American Helicopter Society,* vol. 67, no. 1, pp. 1-17, 2022. DOI: 10.4050/JAHS.67.012011.

[7] R. Healy, M. Misiorowski and F. Gandhi, "CFD-Based Examination of Rotor-Rotor Separation Effects on Interactional Aerodynamics for eVTOL Aircraft," *Journal of the American Helicopter Society,* vol. 61, no. 1, pp. 1-12, 2022. DOI: 10.4050/JAHS.67.012006.

[8] J. Luo, L. Zhu and G. Yan, "Novel quadrotor forward-flight model based on wake interference," *AIAA Journal,* vol. 53, no. 12, pp. 3522-3533, 2015. DOI: 10.2514/1.J053011.

[9] M. Tugnoli, D. Montagnani, M. Syal, G. Droandi and A. Zanotti, "Mid-fidelity approach to aerodynamic simulations of unconventional VTOL aircraft configurations," *Aerospace Science and Technology,* vol. 115, p. 106804, 2021. DOI: 10.1016/j.ast.2021.106804.

[10] S. Yoon, H. C. Lee and T. H. Pulliam, "Computational analysis of multi-rotor flows," in *54th AIAA aerospace sciences meeting*, 2016. DOI: 10.2514/6.2016-0812.

[11] R. Piccinini, M. Tugnoli and A. Zanotti, "Numerical Investigation of the Rotor-Rotor Aerodynamic Interaction for eVTOL Aircraft Configurations," *Energies,* vol. 13, no. 22, p. 5995, 2020, DOI: 10.3390/en13225995.

[12] D. Usov, W. Appleton, A. Filippone and N. Bojdo, "Low-Order Aerodynamic Model for Interference in Multi-Rotor Systems," *Journal of Aircraft,* vol. 0, no. 0, pp. 1-13, 2022, DOI: 10.2514/1.C036797.

[13] J. G. Leishman, "Rotor Wakes and Blade Tip Vortices," in *Principles of Helicopter Aerodynamics*, New York, Cambridge University Press, 2006, pp. 567-655.

[14] F. D. Harris, "Hover performance of isolated proprotors and propellers-experimental data," No. NASA/CR-2017-219486, 2017.

[15] W. Johnson, Helicopter theory, New York: Dover Publications, 1994.

[16] G. J. Leishman, "Aerodynamics of Rotor Airfoils," in *Principles of Helicopter Aerodynamics*, New York, Cambridge University Press, 2006, pp. 347-423.

[17] D. E. Goldberg, Genetic Algorithms in Search, Optimization & Machine Learning, Addison-Wesley, 1989.

[18] M. Clerc, Particle swarm optimization, John Wiley & Sons, 2010.

[19] W. Johnson, G. Yamauchi, M. Derby and A. Wadcock, "Wind Tunnel Measurements and Calculations of Aerodynamic Interactions Between Tiltrotor Aircraft," in *41st Aerospace Sciences Meeting and Exhibit*, Reno, NV, 2003.

[20] Leonardo Helicopters, "The UK Vertical Lift Network and the Mentor Project," in *47th European Rotorcraft Forum*, Glasgow, 2021.

APPENDIX

Table 2: Randomly generated tri-rotor configurations.

Configuration	***Hub x_i/R***	***Hub y_i/R***
1	-d, 0	d, -d
2	0, d	d, -d
3	d, d	d, -d
4	d, 0	-d, d
5	0, -d	d, 0
6	d, -d	-d, -d
7	d, 0	-d, -d
8	d, 0	0, d
9	0, d	-d, -d
10	d, -d	0, d
11	-d, -d	-d, 0
12	d, d	-d, 0

Table 3: Randomly generated tetra-rotor configurations.

Configuration	***Hub x_i/R***	***Hub y_i/R***
1	2d, 2d, -d	-d, -2d, d
2	2d, -d, d	-2d, -d, d
3	d, d, 0	-d, d, d
4	2d, 2d, 0	0, -2d, -d
5	-d, 0, 0	d, d, -2d
6	-d, 2d, d	-d, -d, -2d
7	-d, d, 2d	-2d, d, 0
8	2d, -d, -d	d, -2d, 0
9	2d, -d, -d	-d, d, 0
10	2d, d, 2d	0, -d, -d
11	-d, -d, d	-2d, 0, -d
12	2d, d, -d	0, 0, -2d

Presented at 48th European Rotorcraft Forum, Switzerland, 6-8th September, 2022